LIMNOLOGY and OCEANOGRAPHY

ASLO

Limnol. Oceanogr. 67, 2022, 946–961

doi: 10.1002/lno.12047

Light absorption spectra of naturally mixed phytoplankton assemblages for retrieval of phytoplankton group composition in coastal oceans

Xuerong Sun [1], **Fang Shen** [1*], **Robert J.W. Brewin** [2], **Mengyu Li** [1], **Qing Zhu** [1]

[1]State Key Laboratory of Estuarine and Coastal Research, Center for Blue Carbon Science and Technology, East China Normal University, Shanghai, China

[2]Centre for Geography and Environmental Science, College of Life and Environmental Sciences, University of Exeter, Cornwall, UK

Abstract

Phytoplankton group composition is complex and highly variable in coastal waters. Given that different taxonomic groups have different pigment signatures, which in turn impact the light absorption spectra of phytoplankton, the absorption spectral-based approach has the potential for distinguishing phytoplankton groups. Using a large dataset of in situ surface observations of concurrent HPLC (high-performance liquid chromatography) pigments and phytoplankton absorption spectra collected from 2015 to 2018 in Chinese coastal oceans, in situ phytoplankton group composition was obtained from chemotaxonomic analysis (CHEMTAX). By using the linear additive principle on phytoplankton absorption spectra and CHEMTAX results, the chlorophyll-specific absorption spectra of eight phytoplankton groups were reconstructed, including prasinophytes, dinoflagellates, cryptophytes, chlorophytes, cyanobacteria, diatoms, chrysophytes, and prymnesiophytes. These chlorophyll-specific absorption spectra were subsequently used as inputs to a spectral-based inversion model for estimating phytoplankton group composition from the phytoplankton absorption coefficient. The optimal band selection and initial guesses of the phytoplankton group composition, derived from correlation and HCA (hierarchical cluster analysis) analyses, were included in the model inversion to improve the accuracy of retrievals. The performance of the proposed model was validated using an independent dataset, showing accurate estimates of chlorophyll *a* (Chl *a*) concentrations for seven phytoplankton groups ($0.371 \le r \le 0.721$, $p < 0.05$), apart from chrysophytes. Our results suggest that the absorption spectral-based approach is able to discriminate phytoplankton group composition quantitatively, which has implications for retrieving Chl *a* concentrations of phytoplankton groups from hyperspectral platforms and satellites.

Phytoplankton are responsible for nearly half of global net primary production and play a key role in modulating the Earth's climate (Field et al. 1998; Falkowski 2012). Among the diverse communities of phytoplankton present in the sea, some species have similar morphological and physiological characteristics, or share similar ecological and biogeochemical functions, which have been classified into phytoplankton functional types (Nair et al. 2008; IOCCG 2014). Phytoplankton diversity is high across the ocean, and their composition changes with time and space, tightly related to local environmental and global climatic changes (Brewin et al. 2012; Mouw et al. 2019). Phytoplankton composition is considered an ecological indicator that can be used for tracking the health of the ocean, with implications for understanding biogeochemical processes and for marine management (Hays et al. 2005; Platt and Sathyendranath 2008).

Given this importance, great efforts have been made to improve the in situ detection and measurement of phytoplankton composition (Lombard et al. 2019). Pigments derived from high performance liquid chromatography (HPLC) have become the most common way to study phytoplankton biomass and diversity, and are recognized as the standard measurement for the calibration and validation of some ocean color products (Jeffrey et al. 2012; IOCCG 2014). Some pigments or pigment groups are chemotaxonomic markers for specific phytoplankton types and have formed the basis for deriving phytoplankton size structure and taxonomic composition from pigment

*Correspondence: fshen@sklec.ecnu.edu.cn

Additional Supporting Information may be found in the online version of this article.

Author Contribution Statement: Fang Shen is responsible for the administration of projects. Xuerong Sun and Fang Shen conceived the study and designed the fieldwork. Xuerong Sun, Mengyu Li and Qing Zhu contributed to the field data and analyzed the field samples in the laboratory. Xuerong Sun performed the data analysis and wrote the original draft. Fang Shen and Robert J.W. Brewin contributed to the writing, reviewing and editing of the manuscript. All authors gave feedback on the manuscript and have approved the final version.

information, such as diagnostic pigment analysis (Vidussi et al. 2001; Uitz et al. 2006; Hirata et al. 2011), and the CHEMTAX approach (Mackey et al. 1996; Higgins et al. 2012). Using matrix factorization and known pigment ratios for each phytoplankton group, CHEMTAX has been applied widely in both the open and coastal oceans for determining taxonomic group composition (Isada et al. 2015; Zhang et al. 2018; Moore and Brown 2020). CHEMTAX has also proven reliable for estimating phytoplankton groups in Chinese coastal waters (Furuya et al. 2003; Zhu et al. 2009), with consistent results to microscopy and flow cytometry observations (Liu et al. 2016).

However, discrete in situ observations are not well suited for monitoring the distribution of phytoplankton groups at synoptic scales and over long time periods. As a result, there have been increasing efforts to estimate phytoplankton group composition using satellite remote sensing of ocean color, including abundance-based, spectral-based, and ecological-based approaches

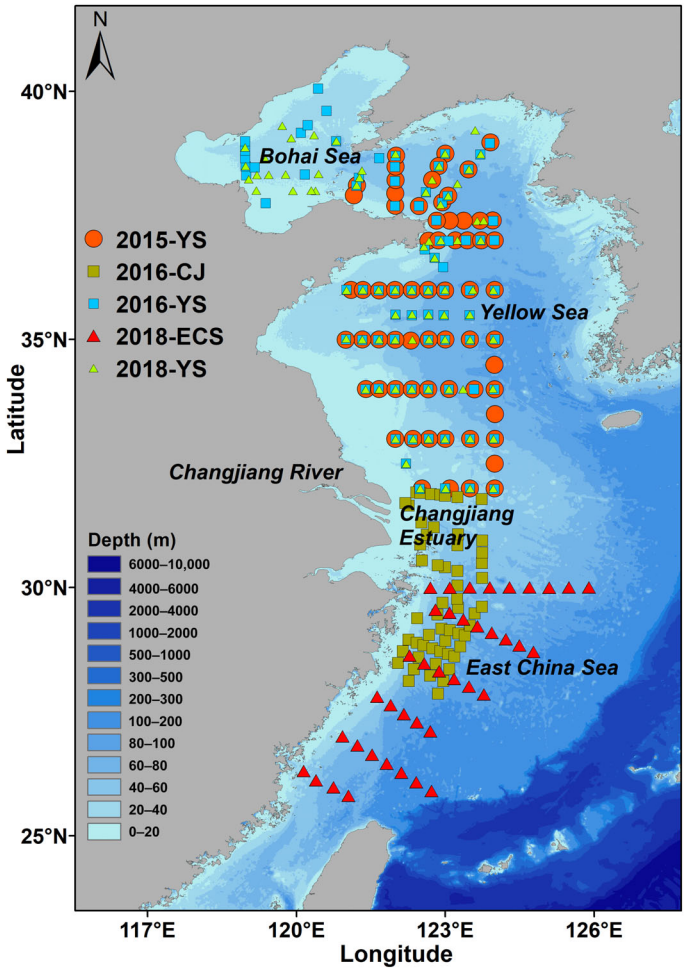

Fig. 1. Sampling locations of the in situ dataset. The abbreviations YS, CJ, and ECS represent the Bohai Sea and Yellow Sea, Changjiang Estuary and adjacent area, and East China Sea, respectively. The background coastline (the GSHHG, version 2.3.7) and bathymetry (the GEBCO 2021 Grid) maps are from NOAA (https://www.ngdc.noaa.gov/mgg/shorelines/) and GEBCO (http://www.gebco.net/), respectively.

(Nair et al. 2008; Brewin et al. 2011; IOCCG 2014). Since variations in the spectral absorption coefficient of phytoplankton have been related to changes in phytoplankton community structure and biomass (Hoepffner and Sathyendranath 1991; Bricaud et al. 2004), and considering there are models developed to retrieve the phytoplankton absorption coefficient from satellite data, absorption-based approaches are increasingly being developed for retrieving phytoplankton information, such as pigment content (Chase et al. 2017; Moisan et al. 2017; Liu et al. 2019), phytoplankton size classes (Hirata et al. 2008; Devred et al. 2011), and phytoplankton group composition (Zhang et al. 2018). In recent years, hyperspectral absorption data have been used to improve the accuracy of retrievals of phytoplankton functional types, utilizing techniques like spectral decomposition, derivative analysis, and hierarchical cluster analysis (Torrecilla et al. 2011; Uitz et al. 2015; Zhang et al. 2015).

The Bohai Sea, Yellow Sea, and East China Sea are three marginal seas located in the northwestern Pacific Ocean off the east coast of China. Under strong influences from rivers (e.g., Changjiang River), tides, ocean currents, and seasonal monsoons, these waters are characterized by high levels of particulates and colored dissolved organic matter (Shi and Wang 2012). Various taxonomic groups of phytoplankton have been identified in this optically-complex environment through microscopy (Guo et al. 2014; Liu et al. 2015a; Jiang et al. 2019), with diatoms the most dominant group in cell abundance, and dinoflagellates, prasinophytes, cryptophytes, chlorophytes, cyanobacteria, chrysophytes, and prymnesiophytes frequently reported as well. However, few studies have assessed the relationships between phytoplankton absorption spectra and phytoplankton group composition in the region, and the feasibility of using absorption-based approaches for phytoplankton group composition retrievals remains limited in the study area.

The aim of this study is to assess whether a matrix inversion method is capable of retrieving the chlorophyll *a* (Chl *a*) concentration of eight phytoplankton groups from phytoplankton absorption spectra. The matrix inversion model is tuned and validated using a large in situ dataset collected during five research cruises over a 3-yr period. The chlorophyll-specific absorption coefficients of eight phytoplankton groups are retrieved and compared with those from laboratory cultures (Clementson and Wojtasiewicz 2019a) and field data (Brewin et al. 2019). The optimal band selection and an initial guess of phytoplankton group composition are introduced as constraints to optimize the matrix inversion model. We evaluate the performance of the model and test its capability to retrieve phytoplankton group composition in coastal oceans.

Data and methods

Cruise information and water sampling

A total of 320 concurrent in situ surface samples for measurements of phytoplankton pigment concentrations and particulate absorption spectra were collected during five research

cruises from 2015 to 2018 in the Bohai Sea, Yellow Sea, and East China Sea (Fig. 1; Supplementary Table S1). Among the whole dataset, 256 samples (i.e., 80%) were selected randomly as the training dataset, leaving 64 independent samples (i.e., 20%) for validation.

Surface water was collected from a depth of around 3 m, using Niskin bottles equipped with a conductivity-temperature-depth profiler (CTD, Seabird 911) rosette. For both pigment concentrations and particulate absorption spectra samples, seawater (100–3000 mL) was filtered onto Whatman GF/F Glass Microfiber Filters (0.7 μm, 25 mm) under low vacuum pressure onboard, and stored in the -40°C refrigerator or in liquid nitrogen until analysis when back at the laboratory, following the NASA ocean optics protocols (Bidigare et al. 2003; Mitchell et al. 2003).

HPLC pigments and CHEMTAX analysis

Phytoplankton pigment concentrations derived from HPLC were analyzed following the methods of Zhang et al. (2016) for cruises 2015-YS, 2016-CJ, 2018-ECS, and 2018-YS, and of Wang et al. (2016) for cruise 2016-YS. The HPLC analysis provided concentrations of Chl *a* (representing the sum of monovinyl Chl *a* and divinyl Chl *a*) and 11 diagnostic pigments (i.e., peridinin, 19′-butanoyloxyfucoxanthin, fucoxanthin, neoxanthin, prasinoxanthin, 19′-hexanoyloxyfucoxanthin, violaxanthin, alloxanthin, zeaxanthin, lutein, and chlorophyll *b*). Some of these pigments are biomarkers for specific taxonomic groups, which can be used as indicators for those taxa (Jeffrey et al. 2012; Catlett and Siegel 2018), with taxonomic meaning shown in Supplementary Table S2. Values below detection limits and 0.001 mg m^{-3} were set to zero before further analysis to minimize the disagreements for pigments derived from different laboratories (Claustre et al. 2004) and to control the quality of the pigment data (Aiken et al. 2009). The frequency histograms of pigments are shown in Supporting Information Fig. S1. Taking Chl *a* concentration as an example, the $\log_{10}$-scale data follow a normal distribution, ranging from 0.129 to 21.652 mg m^{-3}, with the mean value of 2.478 mg m^{-3}.

By performing the HCA on 11 pigment ratios that were normalized to Chl *a* concentration (Kramer and Siegel 2019), a dendrogram (Supporting Information Fig. S2) was constructed by using the correlation distance algorithm (pdist, "correlation") and the unweighted average distance (linkage, "average") in MATLAB R2019b, with a cophenetic correlation coefficient at 0.820. Based on the taxonomic meaning of diagnostic pigments (Supplementary Table S2), eight phytoplankton groups (i.e., prasinophytes, dinoflagellates, cryptophytes, chlorophytes, cyanobacteria, diatoms, chrysophytes, and prymnesiophytes) were clearly identified by applying the HCA on the pigment dataset.

The Chl *a* and 11 diagnostic pigments were then used as inputs to the CHEMTAX program (version 1.95) to identify and estimate the in situ contribution of each phytoplankton group to total Chl *a* concentration. In this study, the initial pigment ratio matrix used in the CHEMTAX program (Supplementary Table S3) is the same as previous studies (Liu et al. 2015b; Sun et al. 2019a). Considering that pigment ratios might vary within the same study area, we processed the CHEMTAX separately for each cruise to minimize uncertainties due to changes in pigment ratios. Following the instructions packaged with the CHEMTAX program, 60 further ratio matrices were generated and then used as inputs through an iterative process. Finally, the best six runs (i.e., 10%) with the lowest root mean squared error (RMSE) were selected to calculate the average Chl *a* concentrations of eight phytoplankton groups. The five final ratio matrixes for each cruise are shown in Supplementary Tables S4–S8. The frequency histograms of Chl *a* concentrations of eight phytoplankton groups are shown in Supporting Information Fig. S3. In order to ensure the results are meaningful, values of Chl *a* concentration of each phytoplankton group from the CHEMTAX program lower than 0.001 mg m^{-3} were set to zero.

Phytoplankton absorption data and analysis

The optical densities of total and non-algal particles were measured by the inside sphere mode (i.e., IS mode) with a PerkinElmer Lambda 1050 UV/VIS spectrophotometer equipped with a 15-cm integrating sphere, in the range of 200–1000 nm at 2-nm resolution and 1-nm interpolation. The particulate absorption coefficients were computed following the NASA and IOCCG ocean optics protocols (Mitchell et al. 2003; Roesler et al. 2018). The absorption coefficients of total and nonalgal particles, $a_p(\lambda)$ and $a_{\mathrm{NAP}}(\lambda)$, were obtained before and after pigment extraction in methanol respectively, calculated from the optical densities as,

$$a_p(\lambda) \text{ or } a_{\mathrm{NAP}}(\lambda) = \frac{2.303 A_f}{\beta B_f}\left[\mathrm{OD}_{fp}(\lambda) - \mathrm{OD}_{bf}(\lambda)\right] \quad (1)$$

where A_f is the area of the filtration, B_f is the filtration volume, the pathlength amplification factor β is set to 4.5 following Röttgers and Gehnke (2012), and $\mathrm{OD}_{fp}(\lambda)$ and $\mathrm{OD}_{bf}(\lambda)$ are optical densities of the sample filter and the blank filter, respectively. The phytoplankton absorption spectra, $a_{ph}(\lambda)$, were finally determined as the difference $a_p(\lambda) - a_{\mathrm{NAP}}(\lambda)$.

Prior to analysis, $a_{ph}(\lambda)$ were restricted to the visible spectral range of 400–700 nm first, and smoothed using the Savizky–Golay filtering (MATLAB R2019b, sgolayfilt) with polynomial order of 4 and frame length of 21 (Xi et al. 2015). The spectral shape of $a_{ph}(\lambda)$ was obtained by normalizing $a_{ph}(\lambda)$ to the integral over the range of 400–700 nm,

$$a_{ph,n}(\lambda) = a_{ph}(\lambda) \Big/ \int_{400}^{700} a_{ph}(\lambda) d\lambda \quad (2)$$

where n means normalized, and $a_{ph,n}(\lambda)$ represents normalized $a_{ph}(\lambda)$. The chlorophyll-specific absorption, $a^*_{ph}(\lambda)$, was calculated as follows:

$$a^*_{ph}(\lambda) = a_{ph}(\lambda) / C_{\mathrm{HPLC}} \quad (3)$$

where C_{HPLC} is the Chl *a* concentration measured by HPLC method.

In order to enhance the spectral features between samples and provide more diverse optics-based classification clusters, 1st to 4th derivative analyses were further applied to the normalized spectra $a_{ph,n}(\lambda)$, following previous studies (Torrecilla et al. 2011; Isada et al. 2015; Xi et al. 2015),

$$\begin{aligned} a'_{ph,n}(\lambda) &= \frac{a_{ph,n}(\lambda+\Delta\lambda) - a_{ph,n}(\lambda-\Delta\lambda)}{2\Delta\lambda} \\ a''_{ph,n}(\lambda) &= \frac{a_{ph,n}(\lambda+\Delta\lambda) - 2*a_{ph,n}(\lambda) + a_{ph,n}(\lambda-\Delta\lambda)}{\Delta\lambda^2} \\ a'''_{ph,n}(\lambda) &= \frac{a_{ph,n}(\lambda+2*\Delta\lambda) - 2*a_{ph,n}(\lambda+\Delta\lambda) + 2*a_{ph,n}(\lambda-\Delta\lambda) - a_{ph,n}(\lambda-2*\Delta\lambda)}{2\Delta\lambda^3} \\ a''''_{ph,n}(\lambda) &= \frac{a_{ph,n}(\lambda+2*\Delta\lambda) - 4*a_{ph,n}(\lambda+\Delta\lambda) + 6*a_{ph,n}(\lambda) - 4*a_{ph,n}(\lambda-\Delta\lambda) - a_{ph,n}(\lambda-2*\Delta\lambda)}{\Delta\lambda^4} \end{aligned} \quad (4)$$

where the band separation, $\Delta\lambda$, is set at 14 nm, making the spectral range of derivatives 428–672 nm. The justification for the band separation settings can be found in the Supplementary (Supporting Information Fig. S4; Table S9; Text S1).

Hierarchical cluster analysis

The application of HCA on the original and 1st to 4th derivative spectra of $a_{ph,n}(\lambda)$ was used to group the training dataset according to their optical features. The dendrogram was constructed in MATLAB R2019b by calculating the pairwise distance between each pair of observations using the correlation distance algorithm and unweighted average distance. Five dendrograms obtained from the HCA on $a_{ph,n}(\lambda)$ and its 1st to 4th derivatives are shown in Supporting Information Fig. S5. Taking the dendrogram resulting from the original spectra of $a_{ph,n}(\lambda)$ for example (Supporting Information Fig. S5a1), eight clusters were considered for further analysis, based on the relationship between linkage distance and node number (Supporting Information Fig. S5a2). The HCA was applied to the 1st to 4th derivative spectra of $a_{ph,n}(\lambda)$ in the same manner as the original $a_{ph,n}(\lambda)$, leading to 40 clusters in total. However, among all the 40 clusters, many of them contained similar or the same samples and optical properties. Under this circumstance, to solve this issue, we calculated the index $S_{i,j}$ between every two $a^*_{ph}(\lambda)$ of 40 clusters, as described in Zhang et al. (2015),

$$S_{i,j} = \frac{2}{301}\sum_{k=1}^{301}\left|\frac{a^*_{ph,i}(\lambda_k) - a^*_{ph,j}(\lambda_k)}{a^*_{ph,i}(\lambda_k) + a^*_{ph,j}(\lambda_k)}\right| \quad (5)$$

where *i* and *j* represent two specific spectra, *k* represents the wavelength from 400 to 700 nm, and the similarity threshold of $S_{i,j}$ is set at 0.1, below which two spectra could not be distinguished optically (Zhang et al. 2015). Subsequently, we combined every pair of clusters of which $S_{i,j}$ were lower than 0.1, and finally eight clusters were reserved, representing different absorption properties (Fig. 6; Table 1). The justification for using all the original and 1st to 4th derivatives of $a_{ph,n}(\lambda)$ for HCA analysis can be found in Supplementary Text S2.

Matrix inversion analysis

Since the $a_{ph}(\lambda)$ can be expressed as the additive contributions of $a^*_{ph}(\lambda)$ of phytoplankton groups and their corresponding Chl *a* concentrations, matrix inversion analysis can be applied to the reconstruction of $a_{ph}(\lambda)$ for mixed phytoplankton groups (Zhang et al. 2018). In this study, the $a_{ph}(\lambda)$ coefficients were reconstructed as the linear additive contributions of $a^*_{ph}(\lambda)$ of eight individual phytoplankton groups and their corresponding Chl *a* concentrations, according to Eq. 3,

$$a_{ph}(\lambda) = \sum_{i=1}^{n} C_i a^*_i(\lambda) \quad (6)$$

where *i* is phytoplankton group, *n* is the number of different phytoplankton groups, $a^*_i(\lambda)$ and C_i are the chlorophyll-specific absorption and Chl *a* concentration for the i^{th} phytoplankton group, respectively. By dividing the Chl *a* on both sides, Eq. 6 can be further expressed as

$$a^*_{ph}(\lambda) = \sum_{i=1}^{n} f_i a^*_i(\lambda) \quad (7)$$

where f_i is the fraction of total Chl *a* of the i^{th} phytoplankton group.

Chlorophyll-specific absorption of phytoplankton groups

The first matrix inversion was applied to the large number of observed phytoplankton absorption and Chl *a* fractions of eight groups obtained from CHEMTAX in the training dataset, and the unknown chlorophyll-specific absorption of each phytoplankton group, $a^*_i(\lambda)$, was retrieved based on Eq. 7, as follows:

$$\begin{pmatrix} f_{i=1,j=1} & \cdots & f_{i=m,j=1} \\ \vdots & \ddots & \vdots \\ f_{i=1,j=n} & \cdots & f_{i=m,j=n} \end{pmatrix} \begin{pmatrix} a^*_{i=1}(\lambda) \\ \vdots \\ a^*_{i=m}(\lambda) \end{pmatrix} = \begin{pmatrix} a^*_{ph,j=1}(\lambda) \\ \vdots \\ a^*_{ph,j=n}(\lambda) \end{pmatrix} \quad (8)$$

where n is the number of samples in the training dataset ($n = 256$), m is the number of phytoplankton groups ($m = 8$), $f_{i,j}$ is the in situ Chl a fraction of the i^{th} phytoplankton group of the j^{th} sample, and $a^*_{ph,j}(\lambda)$ is chlorophyll-specific absorption of the j^{th} sample at a given wavelength from 400 to 700 nm.

To retrieve the $a^*_i(\lambda)$ for each phytoplankton group, the combination of a constrained linear least-squares solver (MATLAB R2019b, lsqlin) and bootstrapping was used. In brief, we randomly selected a certain number (i.e., from 40 to 250 with an interval of 10, 22 groups in total) of samples from the training dataset ($N = 256$) with the replacement at 1000 times first, and then each group was brought into Eq 8 using the linear least-squares solver with the lower bound ≥ 0, resulting in the final mean and standard deviation of $a^*_i(\lambda)$ of eight phytoplankton groups (*see* the "Retrieved specific absorption of phytoplankton groups" section).

Chl a *concentrations of phytoplankton groups*

Once the resulting $a^*_i(\lambda)$ of eight phytoplankton groups are obtained, they become the known parameters, and along with the observed $a_{ph}(\lambda)$ in the independent validation dataset, Chl a concentration of i^{th} phytoplankton group for the j^{th} sample, $C_{i,j}$, could be estimated. The second matrix inversion analysis is based on Eq. 6, as follows:

$$\begin{pmatrix} a^*_{i=1}(\lambda_1) & \cdots & a^*_{i=m}(\lambda_1) \\ \vdots & \ddots & \vdots \\ a^*_{i=1}(\lambda_L) & \cdots & a^*_{i=m}(\lambda_L) \end{pmatrix} \begin{pmatrix} C_{i=1,j=1\ldots nn} \\ \vdots \\ C_{i=m,j=1\ldots nn} \end{pmatrix} = \begin{pmatrix} a_{ph,j=1\ldots nn}(\lambda_1) \\ \vdots \\ a_{ph,j=1\ldots nn}(\lambda_L) \end{pmatrix} \quad (9)$$

where nn is the number of the samples in the validation dataset ($nn = 64$), and L is the number of wavelengths, which could be the number of selected significant bands of each phytoplankton group (*see* the "Optimal band selection" section), or 301 for the whole range 400–700 nm as a comparison.

To retrieve the Chl a concentrations of the eight phytoplankton groups for a given $a_{ph}(\lambda)$, steps are as follows. Firstly, the pairwise distance between every 2nd derivative of $a_{ph,n}(\lambda)$ in the validation dataset and the 2nd derivative of $a_{ph,n}(\lambda)$ of eight clusters obtained from the HCA on the training dataset were calculated, using the correlation distance algorithm and unweighted average distance. The justification for using the 2nd derivative of $a_{ph,n}(\lambda)$ was described in Supplementary Text S3. Next, the minimum value of the pairwise distance among all the eight clusters was used to determine the cluster to which the sampled absorption spectrum belonged, and at the same time, the initial guess of the Chl a concentration of each group from the determined cluster was obtained (*see* the "Initial guesses from HCA classification results" section). The last step involved estimating Chl a concentrations of eight phytoplankton groups using the chlorophyll-specific absorption coefficients obtained from the first matrix inversion (*see* the "Retrieved specific absorption of phytoplankton groups" section) and the observed absorption spectra (Eq. 9). To do that, we used a constrained linear least-squares solver (MATLAB R2019b, lsqlin) with the lower bound ≥ 0. To improve the accuracy, initial guesses (*see* the "Initial guesses from HCA classification results" section) were included to minimize the fitting with options specified as "trust-region-reflective," and we selected only significant bands (*see* the "Optimal band selection" section). Similar to the in situ CHEMTAX-derived Chl a concentration, $c_{i,j}$ derived from Eq. 9 was set to zero when lower than 0.001 mg m^{-3}. A flowchart of the training and validation procedures is shown in Fig. 2.

Error tests

Considering that Chl a concentrations are distributed log-normally in the ocean, the performance of the proposed model was quantified using the Pearson linear correlation coefficient (r), p-value (p), bias (δ), mean absolute error (MAE), and RMSE, calculated between in situ measurements and model-derived estimates in $\log_{10}$ space, according to

$$r = \frac{1}{N-1}\sum_{i=1}^{N}\left(\frac{\log_{10}C_{i,E} - \mu_{\log_{10}E}}{\delta_{\log_{10}E}}\right)\left(\frac{\log_{10}C_{i,M} - \mu_{\log_{10}M}}{\delta_{\log_{10}M}}\right) \quad (10)$$

$$\delta = \frac{1}{N}\sum_{i=1}^{N}\left(\log_{10}C_{i,E} - \log_{10}C_{i,M}\right) \quad (11)$$

$$\text{MAE} = \frac{1}{N}\sum_{i=1}^{N}\left|\log_{10}C_{i,E} - \log_{10}C_{i,M}\right| \quad (12)$$

$$\text{RMSE} = \left[\frac{1}{N}\sum_{i=1}^{N}\left(\log_{10}C_{i,E} - \log_{10}C_{i,M}\right)^2\right]^{1/2} \quad (13)$$

where N is the number of samples, C is Chl a concentration, E and M represent estimated and measured Chl a concentrations, μ and δ represent mean and standard deviation of variables E and M, respectively. Note that in addition to the validation, correlation coefficients were also included in analyses which contain spectra (e.g., optimal band selection), where variables were calculated in linear space.

Results and discussion

Retrieved specific absorption of phytoplankton groups

The retrieved mean value and standard deviation of $a^*_{ph}(\lambda)$ of eight phytoplankton groups, calculated from fitting Eq. 8 to

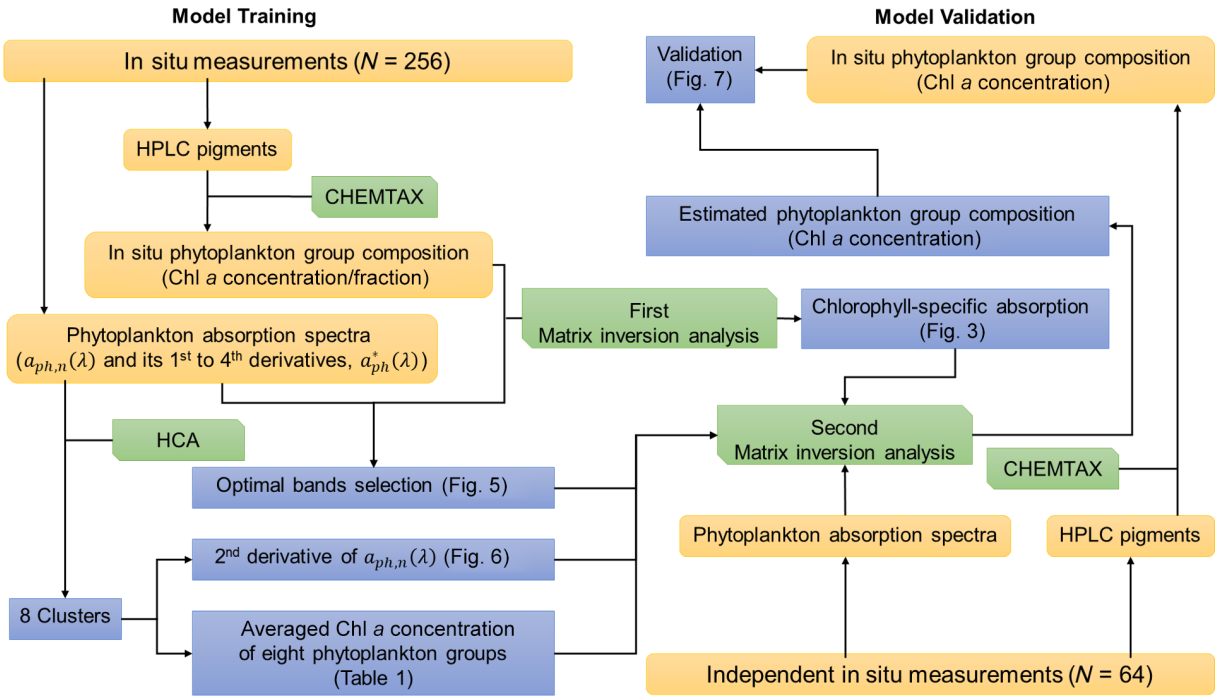

Fig. 2. A flowchart of the datasets and processing procedures in this study. Rounded yellow rectangles represent inputs, diagonal green rectangles represent processes, and blue rectangles represent outputs.

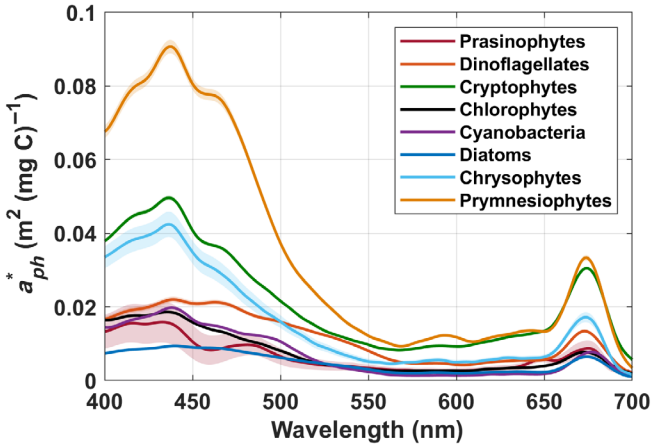

Fig. 3. Chlorophyll-specific absorption coefficients of eight phytoplankton groups derived from the matrix inversion, based on the training dataset ($N = 256$). Solid lines and lighter shades represent the mean value and the standard deviation of the results from 22 groups, respectively.

the training dataset, are shown in Fig. 3. In general, the $a^*_{ph}(\lambda)$ of all groups exhibit two typical peaks of Chl *a* pigment around 440 and 675 nm. Different phytoplankton groups show diversity in the spectral shape of $a^*_{ph}(\lambda)$, which result from the influence of different diagnostic pigments (Bricaud et al. 2004; Clementson and Wojtasiewicz 2019b), as shown in Supporting Information Fig. S6. Prasinophytes exhibit a unique spectral shape in the blue spectral region with two additional peaks at 415 and 475 nm, which may be associated with the pigments neoxanthin, lutein, prasinoxanthin, and violaxanthin, while the peak at 650 nm is likely influenced by chlorophyll *b*. The presence of an additional peak at 465 nm for dinoflagellates may be caused by pigments such as peridinin and alloxanthin. A shoulder peak around 465 nm is observed in cryptophytes, cyanobacteria, and prymnesiophytes, which are likely the result of absorption by pigments alloxanthin, zeaxanthin, and chlorophyll c_2, respectively. Chlorophyll c_2 may be the reason for the small absorption peaks at 580 nm for both cryptophytes and prymnesiophytes.

Regarding magnitude, prymnesiophytes have the highest $a^*_{ph}(\lambda)$ value and the steepest slope among all phytoplankton groups, with the blue-to-red ratio (i.e., 440/675 nm) at 2.71, followed by cyanobacteria at 2.57. In contrast, diatoms show the lowest value and the flattest slope with the blue-to-red ratio at 1.46, and the remaining groups are between diatoms and prymnesiophytes. The changes in blue-to-red ratio are related to changes in pigment composition and the package effect, due to the cell size (Hoepffner and Sathyendranath 1991; Bricaud et al. 2004), such that large cells (small cells) tend to exhibit low (high) chlorophyll-specific absorption and the flattest (steepest) spectral shape. The shaded areas indicate that by selecting different numbers of concurrent measurements (i.e., from 40 to 250 with an interval of 10) in the matrix inversion analysis, the corresponding fitting results are slightly different, especially for prasinophytes, chrysophytes, and prymnesiophytes, and the

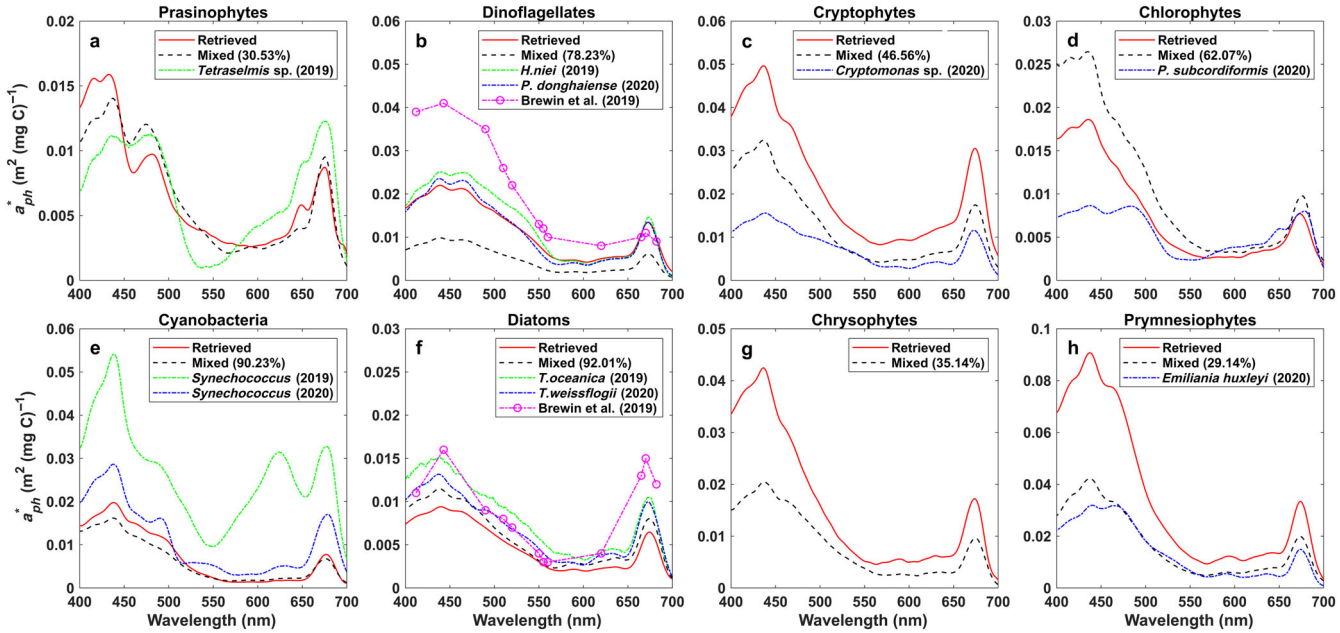

Fig. 4. Comparison of retrieved chlorophyll-specific absorption of phytoplankton groups (red lines) with those of the first four in situ samples with the highest percentages of the corresponding phytoplankton group (black dashed lines, labeled mixed, bracketed values refer to percentages), unialgal cultures (green lines, labeled algae species and 2019) from Clementson and Wojtasiewicz (2019a), unialgal cultures from our research group (unpublished data, blue lines, labeled algae species and 2020), and four-population model retrievals (pink dots) from Brewin et al. (2019), for groups prasinophytes (a), dinoflagellates (b), cryptophytes (c), chlorophytes (d), cyanobacteria (e), diatoms (f), chrysophytes (g), and prymnesiophytes (h).

standard deviations are usually higher in the blue spectral region than those in the red region.

Here, we compared the retrieved $a^*_{ph}(\lambda)$ with that from: (1) the first four in situ samples with the highest percentages of the corresponding phytoplankton group, (2) unialgal cultures of Clementson and Wojtasiewicz (2019a), (3) unialgal cultures from our research group (unpublished data), and (4) the four-component model of Brewin et al. (2019), as shown in Fig. 4. The mean values of in situ $a^*_{ph}(\lambda)$ of the mixed phytoplankton assemblages with the first four most dominant phytoplankton percentages (labeled mixed) were used to evaluate the retrieved $a^*_{ph}(\lambda)$, and high correlation coefficients were observed, ranging from 0.970 to 0.998 at all wavelengths (400–700 nm) for eight groups, indicating that the matrix inversion analysis is able to partition the absorption spectra into the contributions of the eight phytoplankton groups. The correlation coefficients are the highest for dinoflagellates and cyanobacteria (0.998), followed by diatoms (0.995), since high Chl *a* concentrations of these phytoplankton groups were frequently observed during in situ investigations (Supporting Information Fig. S3), which are useful for isolating the $a^*_{ph}(\lambda)$ from naturally mixed assemblages.

For the two most common phytoplankton groups (i.e., dinoflagellates and diatoms) in the study area (Guo et al. 2014; Liu et al. 2015b; Jiang et al. 2019), agreements were found between our inversion results and other studies (Fig. 4b,f). The retrieved $a^*_{ph}(\lambda)$ of dinoflagellates show good agreement with both unialgal cultures measurements in green and red spectral regions of the spectrum, while larger differences are seen between the retrievals and the four-population model in the blue spectral region. Its shape is similar to those from unialgal cultures (i.e., two peaks in the blue spectral region), especially to the *Prorocentrum donghaiense*, which is a very common species in the Changjiang Estuary area and East China Sea (Lu et al. 2005). The values of retrieved $a^*_{ph}(\lambda)$ of diatoms are close to both unialgal culture measurements, while the four-population model estimates are slightly higher in the red spectral region. The retrieved cyanobacteria $a^*_{ph}(\lambda)$ values match those of *Synechococcus* from our research group (Fig. 4e), but are much lower than those from Clementson and Wojtasiewicz (2019a). By comparing with the unialgal species *Tetraselmis* sp. taken from Clementson and Wojtasiewicz (2019a), the retrieved $a^*_{ph}(\lambda)$ of prasinophytes in this study could reflect some characteristics of unialgal cultures, including two specific peaks in the blue spectral region and a peak around 650 nm. As for groups cryptophytes, chlorophytes, and prymnesiophytes, unialgal cultures from our research group were included for comparison, and differences were observed in both magnitude and shape.

In addition to the accuracy of the representation of phytoplankton groups by certain unialgal cultures, differences in $a^*_{ph}(\lambda)$ of phytoplankton groups among various studies are due to the methods used to obtain $a^*_{ph}(\lambda)$. In this study, we used concurrent Chl *a* concentrations of phytoplankton groups derived from CHEMTAX and the phytoplankton absorption coefficient to derive $a^*_{ph}(\lambda)$ of each phytoplankton group

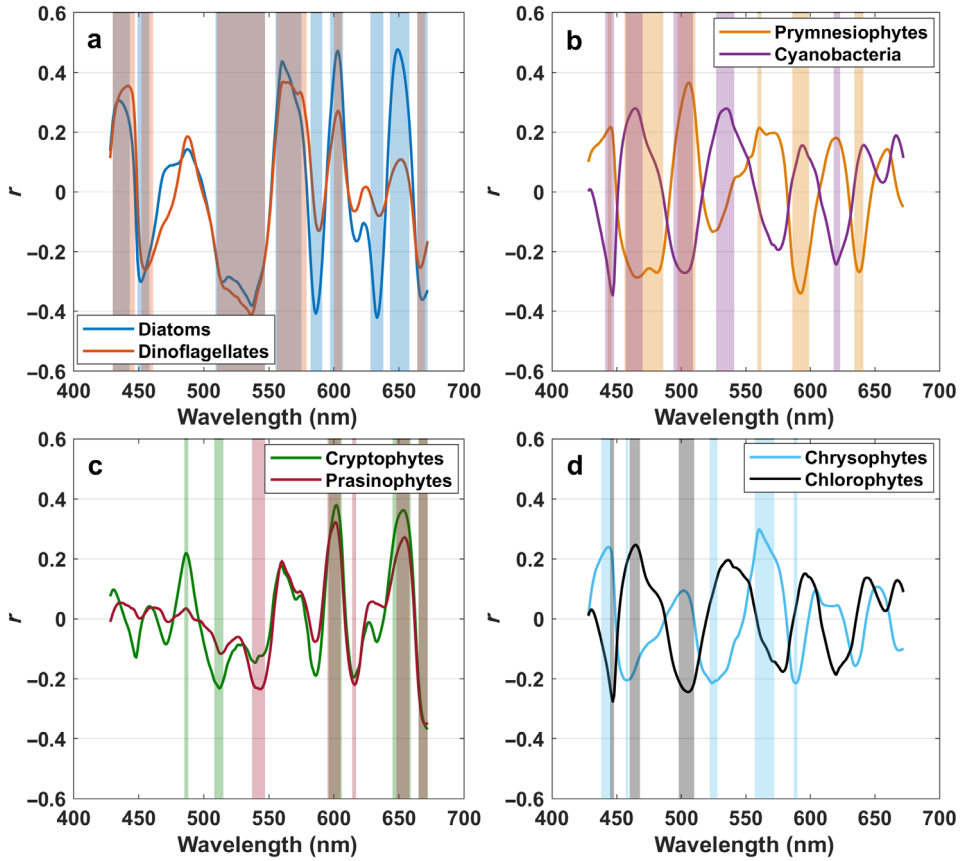

Fig. 5. Correlations between Chl *a* concentration and 2nd derivative of normalized phytoplankton absorption spectra, for diatoms and dinoflagellates (**a**), prymnesiophytes and cyanobacteria (**b**), cryptophytes and prasinophytes (**c**), and chrysophytes and chlorophytes (**d**). The shaded areas represent wavelengths with significant correlations, where $p < 0.001$.

through a linear matrix inversion algorithm. CHEMTAX has a proven capability to derive reliable phytoplankton group composition in eastern China seas (Furuya et al. 2003; Liu et al. 2015b; Sun et al. 2019a). In addition to phytoplankton groups, the matrix inversion analysis has been widely used and is capable of estimating Chl *a* concentration of phytoplankton size classes (Zhang et al. 2015; Brewin et al. 2019) and diagnostic pigments (Moisan et al. 2017; Liu et al. 2019). The cultured algae species from our research group are common species isolated from samples in the study area, which were taken from Shanghai Guangyu Biological Technology Company. The culture experiments were described in a recent study (Shen et al. 2019), with absorption coefficients measured consistently, following "Phytoplankton absorption data and analysis" section. The magnitude and shape of cultured $a^*_{ph}(\lambda)$ vary with the changes in phytoplankton cell size and pigment composition, which are consistent with previous studies (Organelli et al. 2017; Zhou et al. 2017). However, as a common species in the picoplankton size class, $a^*_{ph}(\lambda)$ of *Synechococcus* in our study area is not as high as expected, when compared with that from Clementson and Wojtasiewicz (2019-a), indicating that $a^*_{ph}(\lambda)$ of unialgal cultures may be related to geographical differences, culturing conditions, and absorption protocols. The $a^*_{ph}(\lambda)$ of diatoms derived from the four-population model of Brewin et al. (2019) is comparable with our retrieved result, especially when considering SST is an additional input in their $a^*_{ph}(\lambda)$ retrieval procedure, and their focus is in a different region (i.e., North Atlantic).

Improvements for matrix inversion analysis based on relationships between phytoplankton groups and absorption spectra

Optimal band selection

In order to improve the accuracy of retrievals, relationships between concurrent Chl *a* concentrations of phytoplankton groups and the 2nd derivatives of the $a_{ph,n}(\lambda)$ in the spectral range of 428–672 nm from the training dataset were examined, as shown in Fig. 5, where wavelengths with significant correlation coefficients ($p < 0.001$) are shown with shaded areas.

The number and position of shaded wavelengths are different for eight phytoplankton groups. Diatoms and dinoflagellates have a large number of wavelengths with significant correlations (i.e., 141 and 104), and they are distributed widely in the whole spectrum. Prymnesiophytes and cyanobacteria have 76 and 59 wavelengths, which are distributed

mainly in blue and yellow spectral regions, and blue and green spectral regions, respectively. While for cryptophytes and prasinophytes, significant wavelengths are mainly observed at longer wavelengths, with the numbers 46 and 45, respectively. In contrast, the chrysophytes and chlorophytes have fewer significant wavelengths (i.e., 39 and 26), which are located within 438–590 nm and 445–510 nm, respectively.

Compared to the standard one, the 2nd derivative spectrum is useful for providing qualitative identification of pigments (Bidigare et al. 1989), and has better results in discriminating phytoplankton groups (Uitz et al. 2015), indicating that wavelengths with significant correlation coefficients derived from 2nd derivative analysis of $a_{ph,n}(\lambda)$ and the chlorophyll concentrations may carry the most information on the individual phytoplankton group. Therefore, these wavelengths are consequently selected as the optimal bands for the matrix inversion on the validation dataset.

Initial guesses from HCA classification results

In addition to the selection of optimal bands during the matrix inversion analysis, an initial value was introduced as a priori knowledge to minimize the linear least-squares fitting and improve the accuracy of the inversion. The initial guesses are the mean values of Chl *a* concentration of each phytoplankton group from the eight HCA-derived clusters, as shown in Table 1. The resulting eight clusters here could be explained by the differences in phytoplankton absorption spectra with respect to the group composition.

Taking cluster 2 as an example, which is equivalent to the whole training dataset ($N = 256$), the study area is composed of different phytoplankton groups, with diatoms and cyanobacteria having the highest percentages. Diatoms are the most dominant in six clusters (i.e., clusters 1, 2, 3, 4, 5, and 8) in terms of the Chl *a* concentration. While in the remaining clusters 6 and 7, cyanobacteria have the highest proportions, followed by chlorophytes. Cyanobacteria and chlorophytes in cluster 7 are dominant groups and have higher averaged concentrations than those in cluster 6, resulting in correspondingly higher values of $a_{ph}(\lambda)$ (Fig. 6a). In comparison, the spectral shape of origin and 2nd derivative of $a_{ph,n}(\lambda)$ for clusters 4, 5, and 8 have large differences (Fig. 6b,d), which are related to their phytoplankton composition. Cluster 4 has the highest proportions of dinoflagellates among eight clusters, and its absorption spectrum has an additional peak around 465 nm, consistent with the absorption characteristics of dinoflagellates (Fig. 3). Prymnesiophytes are the second dominant group in cluster 5 and have the highest proportions among the eight clusters. The absorption spectrum of cluster 8 shows similarities with the $a^*_{ph}(\lambda)$ of prasinophytes (Fig. 3), which is consistent with the fact that prasinophytes are the second most dominant group in cluster 8.

Retrieval and validation of concentrations of phytoplankton groups

Using the independent validation dataset ($N = 64$), the performance of the retrieval algorithm was evaluated and compared with the phytoplankton group composition derived from CHEMTAX analysis. As described in the "Chl *a* concentrations of phytoplankton groups" section, the Chl *a* concentration of each phytoplankton group was estimated by applying the matrix inversion model (Eq. 9) to the observed absorption spectra, along with the chlorophyll-specific absorption derived from the "Retrieved specific absorption of phytoplankton groups" section, optimal band selection from the "Optimal band selection" section, and initial guesses from the "Initial guesses from HCA classification results" section (Fig. 2).

Modeled Chl *a* concentrations of the eight phytoplankton groups were plotted against the in situ data, together with the results of error statistics, in Fig. 7. In general, Chl *a* concentrations derived from absorption spectra compare reasonably well with in situ observations. High correlation coefficients (r) are observed in seven groups with p-values below

Table 1. Mean values of total and each phytoplankton group's Chl *a* concentration in eight clusters derived from the HCA (units of mg m^{-3}). Numbers in brackets are the mean percentages of each phytoplankton group (units of %). The two groups with the highest percentages for each cluster are shown in bold, and the cluster with the highest percentage for each group is shown in italics.

Groups/clusters	Cluster 1 ($N = 6$)	Cluster 2 ($N = 256$)	Cluster 3 ($N = 9$)	Cluster 4 ($N = 2$)	Cluster 5 ($N = 22$)	Cluster 6 ($N = 23$)	Cluster 7 ($N = 15$)	Cluster 8 ($N = 4$)
Prasinophytes	0.159 (5.55)	0.090 (4.20)	0.302 (4.74)	0.028 (2.33)	0.059 (2.66)	0.048 (3.57)	0.042 (3.41)	***0.317 (26.99)***
Dinoflagellates	0.370 (5.83)	0.333 (8.58)	0.192 (3.88)	***0.258 (19.65)***	0.103 (5.59)	0.020 (1.43)	0.011 (0.82)	0.008 (0.72)
Cryptophytes	***0.288 (27.23)***	0.164 (7.76)	**0.641 (16.94)**	0.141 (11.89)	0.162 (7.69)	0.082 (5.84)	0.243 (2.71)	0.226 (16.64)
Chlorophytes	0.182 (14.66)	0.254 (14.90)	0.278 (10.59)	0.123 (11.00)	0.099 (8.35)	**0.147 (27.60)**	***1.257 (34.77)***	0.011 (1.10)
Cyanobacteria	0.102 (8.30)	**0.329 (19.91)**	0.086 (2.87)	0.010 (0.84)	0.145 (12.44)	**0.172 (33.25)**	***1.846 (50.72)***	0.085 (7.31)
Diatoms	**1.066 (29.75)**	**1.138 (32.02)**	***4.013 (59.10)***	**0.648 (52.62)**	**1.066 (37.35)**	0.364 (15.11)	0.060 (2.32)	**0.373 (37.46)**
Chrysophytes	0.025 (2.47)	0.078 (5.18)	0.032 (1.06)	0.007 (0.56)	*0.152 (9.61)*	0.091 (4.52)	0.035 (1.99)	0.030 (2.86)
Prymnesiophytes	0.079 (6.21)	0.098 (7.44)	0.046 (0.83)	0.015 (1.10)	***0.354 (16.31)***	0.187 (8.67)	0.059 (3.26)	0.080 (6.92)
Total	2.270	2.484	5.590	1.230	2.141	1.112	3.554	1.131

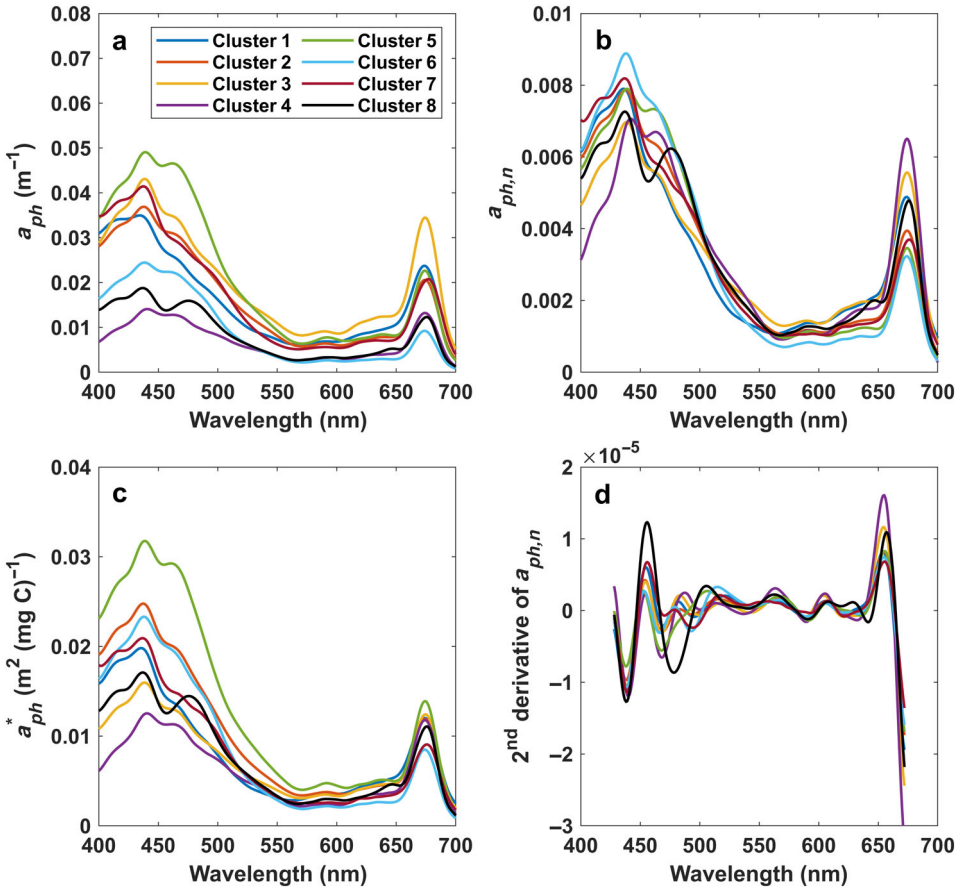

Fig. 6. Mean values of the phytoplankton absorption coefficient (**a**), the normalized phytoplankton absorption coefficient (**b**), the chlorophyll-specific phytoplankton absorption coefficient (**c**), and the 2nd derivative of normalized phytoplankton absorption coefficient (**d**), for eight clusters derived from HCA.

0.05, except for chrysophytes. Diatoms and dinoflagellates have the highest correlation coefficients of 0.721 and 0.606 (Fig. 7b,f), and the MAE and RMSE are lower for diatoms (0.490 and 0.656), indicating that the model has better performance for diatoms. Due to the influence of a few outliers at low Chl *a* concentrations between 0.01 and 1.0 mg m^{-3}, correlation coefficients are relatively low for cyanobacteria and cryptophytes. However, most points are near to the 1 : 1 line (Fig. 7c,e), resulting in the lowest bias for cyanobacteria (−0.043), and a low MAE and RMSE for both cyanobacteria and cryptophytes, relative to other groups. Similarly, the estimated concentrations for prymnesiophytes are in good agreement with the measured results (Fig. 7h), with the lowest MAE and RMSE among eight groups (0.383 and 0.525). For prasinophytes and chlorophytes, some retrievals are below the 1 : 1 line, resulting in a lower correlation coefficient and higher error for these two groups. The scatter of the data points for chrysophytes suggests that the matrix inversion model does not perform well for this group (Fig. 7g). It should be noted that since the evaluation was performed in $\log_{10}$ space, zero values from both in situ and retrieval data were excluded, resulting in a different number of samples for each phytoplankton group.

Sensitivity analysis and performance comparison for the matrix inversion analysis

Previous studies have demonstrated that the sensitivity of the matrix inversion analysis is related to the ill-conditioning of the linear equations, caused by the similarity of any two vectors in the matrix (Zhang et al. 2015; Liu et al. 2019). Therefore, the similarity index $S_{i,j}$ between every two retrieved $a^*_{ph}(\lambda)$ of eight phytoplankton groups was calculated by Eq. 5 to avoid the problem. Among them, prasinophytes and chlorophytes show the most similar shape and magnitude at longer wavelengths (Fig. 3), with the smallest $S_{i,j}$ at 0.14, since prasinophytes and chlorophytes both belong to green algae and share similar diagnostic pigments (Supplementary Table S2), while diatoms and prymnesiophytes have the biggest differences in magnitude, with the largest $S_{i,j}$ of 1.41. The $S_{i,j}$ values are all over 0.1, indicating that, according to Zhang et al. (2015), each of the eight phytoplankton groups could be distinguished optically from the other one.

The performance of the absorption-based model was evaluated by plotting the in situ measurements of eight phytoplankton groups with retrievals derived from matrix inversions with different inputs, as shown in Supporting Information Fig. S7, Table S10, and Text S4. Similar to Fig. 7,

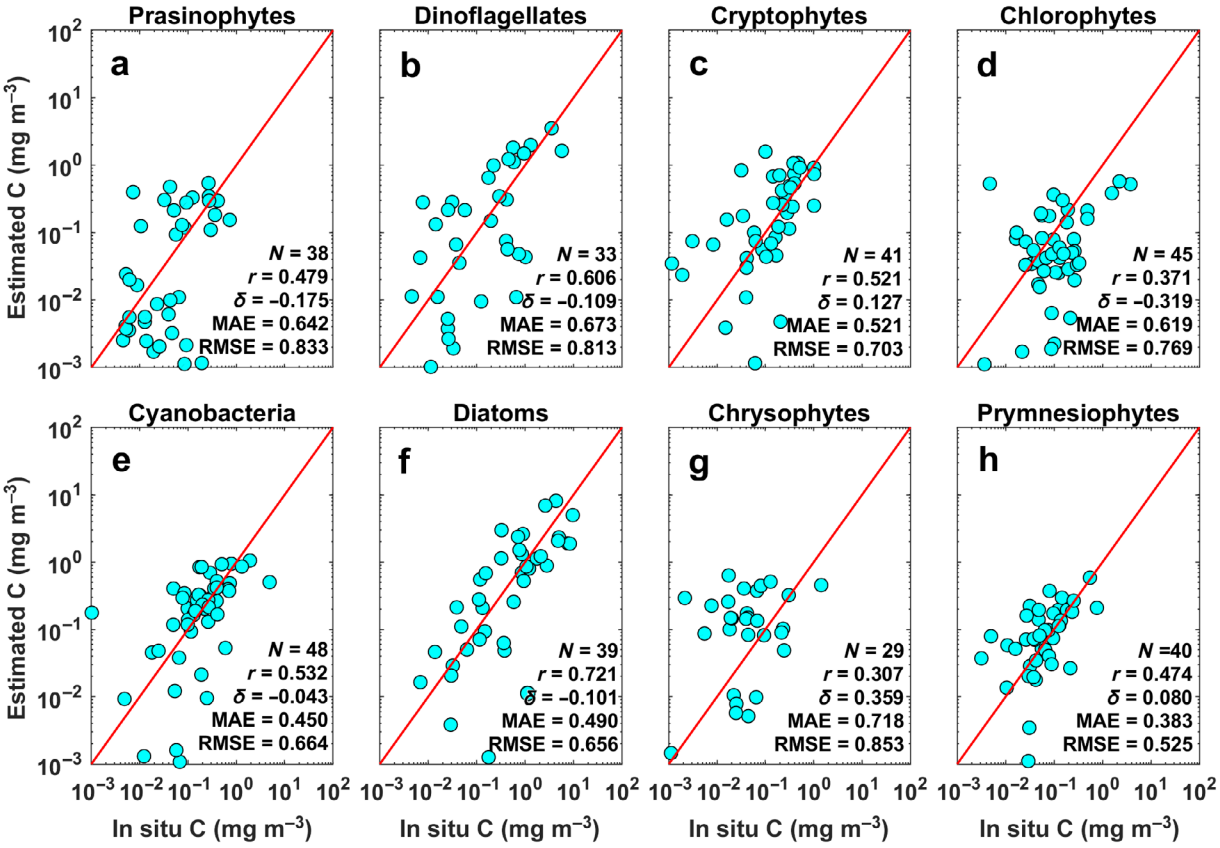

Fig. 7. Independent validation between absorption spectral-based estimates and in situ measurements for the eight phytoplankton groups (**a**–**h**), where Chl *a* denotes the Chl *a* concentration. The solid red line represents the 1 : 1 line. The error statistics are calculated in $\log_{10}$ space.

validation results indicate that dinoflagellates and diatoms have high correlation coefficients, irrespective of inputs (i.e., origin, HCA, bands, or both). As shown in Fig. 4, differences between retrieved results and unialgal measurements from both open and coastal oceans are small, suggesting $a^*_{ph}(\lambda)$ to be relatively stable for different species of dinoflagellates and diatoms. In comparison, due to the high diversity and large size range, intraspecific spectral variabilities of $a^*_{ph}(\lambda)$ were observed for chlorophytes in our unialgal cultures experiments (not shown). This supports the findings from Organelli et al. (2017) that absorption features of chlorophytes vary in natural environments depending on species present, which could explain the low accuracy for chlorophytes in the optical inversion. Results show that retrievals are better when groups have higher contributions to total Chl *a* concentration. In other words, those phytoplankton groups which have a larger influence on $a_{ph}(\lambda)$, such as dinoflagellates, cyanobacteria, and diatoms in this study (Supporting Information Fig. S3), are retrieved with high confidence. Similar relationships between accessory pigments and $a_{ph}(\lambda)$ have been found previously (Moisan et al. 2017), where pigments with a significant contribution to $a_{ph}(\lambda)$ were predicted with the highest accuracy. Therefore, the poor performance for chrysophytes retrievals may be related to its low contribution to total Chl *a* concentration in both training and validation datasets (average 5.18% and 4.92%). The pigment-based classification of phytoplankton groups could be another reason for the low accuracy of the chrysophytes. The violaxanthin, which is used to indicate the presence of chrysophytes (Supporting Information Fig. S2), has been found in multiple taxonomic groups (Jeffrey et al. 2012), highlighting further requirements in evaluating the information in HPLC pigments (Kramer and Siegel 2019).

Since the total $a_{ph}(\lambda)$ is assumed to be the additive contribution of eight phytoplankton groups, the matrix inversion model used in this study is a linear system (Eq. 9). However, when solving the linear least-squares problems with constraints (i.e., lower bound ≥ 0), the problem is always convex, and the solution is global but not necessarily unique. Similar situations have been found in previous studies in solving the nonlinear inversion cases (Roesler and Perry 1995; Zhang et al. 2015; Chase et al. 2017), which illustrates the benefits of introducing an initial guess derived from the HCA. A comparison between the results from the matrix inversion with full bands and that with optimal bands found that using the optimal band selection could increase the number of valid retrievals and improve the accuracy of estimates for some

phytoplankton groups. This is consistent with the findings from previous studies (Torrecilla et al. 2011; Wolanin et al. 2016; Zhang et al. 2018), suggesting that the targeted bands with spectral features could be more important than the spectral resolution (Vandermeulen et al. 2017; Cael et al. 2020).

Implication and limitation of the absorption spectral-based approach

The proposed absorption spectral-based approach in this study shows some advantages over previous work. Firstly, compared with abundance-based models of phytoplankton size classes (Sun et al. 2018, 2019b), it is a more direct approach targeting spectral signatures in $a_{ph}(\lambda)$, and it is capable of retrieving more phytoplankton communities. In addition, it uses the inherent optical properties as input rather than solely Chl *a* concentration, and thus directly relates to optical measurements. The approach could contribute to the knowledge on biogeochemical cycles, for example, by improving optical estimates of primary production (Lee et al. 2015; Sathyendranath et al. 2020), or for assimilating optical data into ecosystem models (Fujii et al. 2007; Skákala et al. 2020). Secondly, efforts have been made recently to develop relationships between continuous underway measurements of hyperspectral absorption coefficients (e.g., AC-S, WETLabs Inc.) and biogeochemical parameters, such as pigments concentrations (Chase et al. 2013; Brewin et al. 2016; Liu et al. 2019), and colored dissolved organic matter absorption (Dall'Olmo et al. 2017). Our approach could be applicable to such data, providing the opportunity to obtain continuous phytoplankton group composition measurements from in situ hyperspectral sensors deployed on research cruises. Finally, as $a_{ph}(\lambda)$ could be estimated from remote sensing reflectance (Werdell et al. 2018), the absorption spectral-based approach could be used to derive phytoplankton group composition from either hyperspectral in situ (e.g., HyperSAS, Sea-Bird Scientific Inc.) or satellite remote sensing reflectance measurements, with the potential to monitor phytoplankton group distributions and dynamics on various time and space scales.

Despite these advantages, there are limitations to this approach. Firstly, the initial pigment ratio matrix of CHEMTAX used in this study (Liu et al. 2015b; Sun et al. 2019a) originated from the knowledge of phytoplankton assemblages in eastern China seas (Furuya et al. 2003). However, pigment ratios may vary as the spatiotemporal distribution of phytoplankton group composition changes, and also due to the differences in physiological states (Schlüter et al. 2000). Even though in situ data were grouped by time interval (i.e., cruise) and run separately in CHEMTAX to minimize the drawbacks of the variation of pigment ratios (Swan et al. 2016; Moore and Brown 2020), comparison with data of taxonomic groups from other methodologies (e.g., microscopy, flow cytometry) is lacking in this study. Secondly, the retrieved $a^*_{ph}(\lambda)$ of each phytoplankton group was derived on a training dataset collected in the past, which might not be representative of conditions in a future ocean. For time series studies, it will be important to ensure continuous collection of in situ measurements for adjusting the $a^*_{ph}(\lambda)$, initial guesses, and optimal band selection. Thirdly, small changes in spectral shape and magnitude of the phytoplankton absorption coefficient could be difficult to detect from ocean color data (Garver et al. 1994), causing difficulties in discriminating phytoplankton groups using the absorption spectral-based approach like that proposed here (Mouw et al. 2017). In addition to phytoplankton, variations in contributions of nonalgal constituents to the total absorption coefficient, backscattering coefficient, and remote sensing reflectance also need to be considered, when applying the proposed absorption spectral-based approach to satellite data. Optically complex coastal waters, where the optical constituents do not co-vary in a predictable manner, are likely to be particularly challenging. Finally, this approach might not be suitable for some commonly used multispectral ocean color sensors, due to the limited number of discrete wavebands available. By testing its application on MODIS (Moderate Resolution Imaging Spectroradiometer) with eight wavelengths in the visible range, with the exception of dinoflagellates, cryptophytes, and chrysophytes, the accuracy and precision decreased for most groups (Supporting Information Fig. S8), highlighting further requirements for hyperspectral imagery, databases, and algorithms (Werdell et al. 2019; Dierssen et al. 2020).

Conclusion

Considering the rising concern for assessing phytoplankton diversity and monitoring its response to environmental and climatic changes, there is an urgent need for developing models for remotely sensed retrieval of phytoplankton group composition. In this study, an absorption spectral-based approach has been proposed for estimating Chl *a* concentration of eight phytoplankton groups (i.e., prasinophytes, dinoflagellates, cryptophytes, chlorophytes, cyanobacteria, diatoms, chrysophytes, and prymnesiophytes) in coastal waters. The $a^*_{ph}(\lambda)$ of eight phytoplankton groups were estimated, which compared reasonably well with spectral signatures of diagnostic pigments, and the $a^*_{ph}(\lambda)$ from previous studies and cultured phytoplankton. Two constraints, optimal band selection and initial guesses, were incorporated in the matrix inversion analysis, which improved the accuracy of estimates. The approach had good performance in retrieving Chl *a* concentrations in dinoflagellates, cryptophytes, cyanobacteria, and diatoms, with high correlation of 0.606, 0.521, 0.532, and 0.721, and RMSE of 0.813, 0.703, 0.664, and 0.656, respectively. Although impacted by several outliers, reasonable errors were found in prasinophytes, chlorophytes, and prymnesiophytes, with a lower correlation of 0.479, 0.371, and 0.474, and RMSE of 0.833, 0.769, and 0.525, respectively. However, the proposed approach had difficulties in retrieving the accurate

concentrations for chrysophytes. Our results demonstrate that phytoplankton group composition can be optically differentiated and quantified using the phytoplankton absorption spectra of naturally mixed phytoplankton assemblage in coastal waters. Even though the application of the proposed absorption spectral-based approach on current ocean color missions with medium spectral resolution is challenging, our approach may be a promising way for application to the next generation of satellites and in situ underway systems equipped with hyperspectral sensors, for exploring the distributions and dynamics of phytoplankton in coastal oceans.

References

Aiken, J., Y. Pradhan, R. Barlow, S. Lavender, A. Poulton, P. Holligan, and N. Hardman-Mountford. 2009. Phytoplankton pigments and functional types in the Atlantic Ocean: A decadal assessment, 1995–2005. Deep-Sea Res. Part II: Top. Stud. Oceanogr. **56**: 899–917. doi:10.1016/j.dsr2.2008.09.017

Bidigare, R. R., J. H. Morrow, and D. A. Kiefer. 1989. Derivative analysis of spectral absorption by photosynthetic pigments in the western Sargasso Sea. J. Mar. Res. **47**: 323–341. doi:10.1357/002224089785076325

Bidigare, R. R., L. Van Heukelem, C. C. Trees, and J. Perl. 2003. HPLC phytoplankton pigments: Sampling, laboratory methods, and quality assurance procedures, p. 5–14. *In* J. L. Mueller, G. S. Fargion, and C. R. McClain [eds.], Ocean optics protocols for satellite ocean color sensor validation, revision 5, volume V: Biogeochemical and bio-optical measurements and data analysis protocols. National Aeronautical and Space Administration.

Brewin, R. J. W., S. Ciavatta, S. Sathyendranath, J. Skákala, J. Bruggeman, D. Ford, and T. Platt. 2019. The Influence of Temperature and Community Structure on Light Absorption by Phytoplankton in the North Atlantic. Sensors **19**: 4182 doi:10.3390/s19194182

Brewin, R. J. W., G. Dall'Olmo, S. Pardo, V. van Dongen-Vogels, and E. S. Boss. 2016. Underway spectrophotometry along the Atlantic Meridional Transect reveals high performance in satellite chlorophyll retrievals. Remote Sens. Environ. **183**: 82–97. doi:10.1016/j.rse.2016.05.005

Brewin, R. J. W., E. Devred, S. Sathyendranath, S. J. Lavender, and N. J. Hardman-Mountford. 2011. Model of phytoplankton absorption based on three size classes. Appl. Opt. **50**: 4535–4549. doi:10.1364/AO.50.004535

Brewin, R. J. W., T. Hirata, N. J. Hardman-Mountford, S. J. Lavender, S. Sathyendranath, and R. Barlow. 2012. The influence of the Indian Ocean Dipole on interannual variations in phytoplankton size structure as revealed by Earth Observation. Deep-Sea Res. Part II: Top. Stud. Oceanogr. **77-80**: 117–127. doi:10.1016/j.dsr2.2012.04.009

Bricaud, A., H. Claustre, J. Ras, and K. Oubelkheir. 2004. Natural variability of phytoplanktonic absorption in oceanic waters: Influence of the size structure of algal populations. J. Geophys. Res. **109**: C11010. doi:10.1029/2004JC002419

Cael, B. B., A. Chase, and E. Boss. 2020. Information content of absorption spectra and implications for ocean color inversion. Appl. Opt. **59**: 3971–3984. doi: 10.1364/AO.389189

Catlett, D., and D. A. Siegel. 2018. Phytoplankton pigment communities can be modeled using unique relationships with spectral absorption signatures in a dynamic coastal environment. J. Geophys. Res.: Oceans **123**: 246–264. doi: 10.1002/2017JC013195

Chase, A., E. Boss, R. Zaneveld, A. Bricaud, H. Claustre, J. Ras, G. Dall'Olmo, and T. K. Westberry. 2013. Decomposition of in situ particulate absorption spectra. Methods Oceanogr. **7**: 110–124. doi:10.1016/j.mio.2014.02.002

Chase, A. P., E. Boss, I. Cetinić, and W. Slade. 2017. Estimation of phytoplankton accessory pigments from hyperspectral reflectance spectra: Toward a global algorithm. J. Geophys. Res.: Oceans **122**: 9725–9743. doi:10.1002/2017JC012859

Claustre, H., and others. 2004. An intercomparison of HPLC phytoplankton pigment methods using in situ samples: Application to remote sensing and database activities. Mar. Chem. **85**: 41–61. doi:10.1016/j.marchem.2003.09.002

Clementson, L. A., and B. Wojtasiewicz. 2019*a*. Dataset on the in vivo absorption characteristics and pigment composition of various phytoplankton species. Data Brief **25**: 104020. doi:10.1016/j.dib.2019.104020

Clementson, L. A., and B. Wojtasiewicz. 2019*b*. Dataset on the absorption characteristics of extracted phytoplankton pigments. Data Brief **24**: 103875. doi:10.1016/j.dib.2019.103875

Dall'Olmo, G., and others. 2017. Determination of the absorption coefficient of chromophoric dissolved organic matter from underway spectrophotometry. Opt. Express **25**: A1079–A1095. doi:10.1364/OE.25.0A1079

Devred, E., S. Sathyendranath, V. Stuart, and T. Platt. 2011. A three component classification of phytoplankton absorption spectra: Application to ocean-color data. Remote Sens. Environ. **115**: 2255–2266. doi:10.1016/j.rse.2011.04.025

Dierssen, H., A. Bracher, V. Brando, H. Loisel, and K. Ruddick. 2020. Data needs for hyperspectral detection of algal diversity across the globe. Oceanography **33**: 74–79. doi:10.5670/oceanog.2020.111

Falkowski, P. 2012. Ocean science: The power of plankton. Nature **483**: S17–S20. doi:10.1038/483S17a

Field, C. B., M. J. Behrenfeld, J. T. Randerson, and P. Falkowski. 1998. Primary production of the biosphere: Integrating terrestrial and oceanic components. Science **281**: 237–240. doi:10.1126/science.281.5374.237

Fujii, M., E. Boss, and F. Chai. 2007. The value of adding optics to ecosystem models: A case study. Biogeosciences **4**: 817–835. doi:10.5194/bg-4-817-2007

Furuya, K., M. Hayashi, Y. Yabushita, and A. Ishikawa. 2003. Phytoplankton dynamics in the East China Sea in spring and summer as revealed by HPLC-derived pigment signatures. Deep-Sea Res. Part II, Top. Stud. Oceanogr. **50**: 367–387. doi:10.1016/S0967-0645(02)00460-5

Garver, S. A., D. A. Siegel, B. Greg, and M. 1994. Variability in near-surface particulate absorption spectra: What can a satellite ocean color imager see? Limnol. Oceanogr. **39**: 1349–1367. doi:10.4319/lo.1994.39.6.1349

Guo, S., Y. Feng, L. Wang, M. Dai, Z. Liu, Y. Bai, and J. Sun. 2014. Seasonal variation in the phytoplankton community of a continental-shelf sea: The East China Sea. Mar. Ecol. Prog. Ser. **516**: 103–126. doi:10.3354/meps10952

Hays, G. C., A. J. Richardson, and C. Robinson. 2005. Climate change and marine plankton. Trends Ecol. Evol. **20**: 337–344. doi:10.1016/j.tree.2005.03.004

Higgins, H. W., S. W. Wright, and L. Schlüter. 2012. Quantitative interpretation of chemotaxonomic pigment data. *In* S. Roy, C. Llewellyn, E. S. Egeland, and G. Johnsen [eds.], Phytoplankton pigments. Cambridge Univ. Press.

Hirata, T., and others. 2011. Synoptic relationships between surface chlorophyll-a and diagnostic pigments specific to phytoplankton functional types. Biogeosciences **8**: 311–327. doi:10.5194/bg-8-311-2011

Hirata, T., J. Aiken, N. Hardman-Mountford, T. J. Smyth, and R. G. Barlow. 2008. An absorption model to determine phytoplankton size classes from satellite ocean colour. Remote Sens. Environ. **112**: 3153–3159. doi:10.1016/j.rse.2008.03.011

Hoepffner, N., and S. Sathyendranath. 1991. Effect of pigment composition on absorption properties of phytoplankton. Mar. Ecol. Prog. Ser. **73**: 11–23. doi:10.3354/meps073011

IOCCG. 2014. *In* S. Sathyendranath [ed.], Phytoplankton functional types from space. International Ocean-Colour Coordinating Group.

Isada, T., T. Hirawake, T. Kobayashi, Y. Nosaka, M. Natsuike, I. Imai, K. Suzuki, and S. Saitoh. 2015. Hyperspectral optical discrimination of phytoplankton community structure in Funka Bay and its implications for ocean color remote sensing of diatoms. Remote Sens. Environ. **159**: 134–151. doi:10.1016/j.rse.2014.12.006

Jeffrey, S. W., S. W. Wright, and M. Zapata. 2012. Microalgal classes and their signature pigments. *In* S. Roy, C. Llewellyn, E. S. Egeland, and G. Johnsen [eds.], Phytoplankton pigments. Cambridge Univ. Press.

Jiang, Z., and others. 2019. Regulation of spatial changes in phytoplankton community by water column stability and nutrients in the Southern Yellow Sea. J. Geophys. Res.: Biogeosci. **124**: 2610–2627. doi:10.1029/2018JG004785

Kramer, S. J., and D. A. Siegel. 2019. How can phytoplankton pigments be best used to characterize surface ocean phytoplankton groups for ocean color remote sensing algorithms? J. Geophys. Res.: Oceans **124**: 7557–7574. doi:10.1029/2019JC015604

Lee, Z., J. Marra, M. J. Perry, and M. Kahru. 2015. Estimating oceanic primary productivity from ocean color remote sensing: A strategic assessment. J. Mar. Syst. **149**: 50–59. doi:10.1016/j.jmarsys.2014.11.015

Liu, H., Y. Huang, W. Zhai, S. Guo, H. Jin, and J. Sun. 2015*a*. Phytoplankton communities and its controlling factors in summer and autumn in the southern Yellow Sea, China. Acta Oceanol. Sin. **34**: 114–123. doi:10.1007/s13131-015-0620-0

Liu, X., and others. 2015*b*. Seasonal phytoplankton response to physical processes in the southern Yellow Sea. J. Sea Res. **95**: 45–55. doi:10.1016/j.seares.2014.10.017

Liu, X., W. Xiao, M. R. Landry, K. Chiang, L. Wang, and B. Huang. 2016. Responses of phytoplankton communities to environmental variability in the East China Sea. Ecosystems **19**: 832–849. doi:10.1007/s10021-016-9970-5

Liu, Y., E. Boss, A. Chase, H. Xi, X. Zhang, R. Röttgers, Y. Pan, and A. Bracher. 2019. Retrieval of phytoplankton pigments from underway spectrophotometry in the Fram Strait. Remote Sensing **11**: 318. doi:10.3390/rs11030318

Lombard, F., and others. 2019. Globally consistent quantitative observations of planktonic ecosystems. Front. Mar. Sci. **6**: 196. doi:10.3389/fmars.2019.00196

Lu, D., J. Goebel, Y. Qi, J. Zou, X. Han, Y. Gao, and Y. Li. 2005. Morphological and genetic study of *Prorocentrum donghaiense* Lu from the East China Sea, and comparison with some related Prorocentrum species. Harmful Algae **4**: 493–505. doi:10.1016/j.hal.2004.08.015

Mackey, M. D., D. J. Mackey, H. W. Higgins, and S. W. Wright. 1996. CHEMTAX - a program for estimating class abundances from chemical markers:application to HPLC measurements of phytoplankton. Mar. Ecol. Prog. Ser. **144**: 265–283. doi:10.3354/meps144265

Mitchell, B. G., M. Kahru, J. Wieland, and M. Stramska. 2003. Determination of spectral absorption coefficients of particles, dissolved material and phytoplankton for discrete water samples. *In* J. L. Mueller, G. S. Fargion, and C. R. McClain [eds.], ocean optics protocols for satellite ocean color sensor validation, revision 4, volume iv: Inherent optical properties: instruments, characterizations, field measurements and data analysis protocols. National Aeronautical and Space Administration.

Moisan, T. A., K. M. Rufty, J. R. Moisan, and M. A. Linkswiler. 2017. Satellite observations of phytoplankton functional type spatial distributions, phenology, diversity, and ecotones. Front. Mar. Sci. **4**; 189. doi:10.3389/fmars.2017.00189

Moore, T. S., and C. W. Brown. 2020. Incorporating environmental data in abundance-based algorithms for deriving phytoplankton size classes in the Atlantic Ocean. Remote Sens. Environ. **240**: 111689. doi:10.1016/j.rse.2020.111689

Mouw, C. B., and others. 2017. A consumer's guide to satellite remote sensing of multiple phytoplankton groups in the global ocean. Front. Mar. Sci. **4**: 41. doi:10.3389/fmars.2017.00041

Mouw, C. B., A. B. Ciochetto, and J. A. Yoder. 2019. A satellite assessment of environmental controls of phytoplankton community size structure. Global Biogeochem. Cycles. **33**: 540–558. doi:10.1029/2018GB006118

Nair, A., S. Sathyendranath, T. Platt, J. Morales, V. Stuart, M. Forget, E. Devred, and H. Bouman. 2008. Remote sensing of phytoplankton functional types. Remote Sens. Environ. **112**: 3366–3375. doi:10.1016/j.rse.2008.01.021

Organelli, E., C. Nuccio, L. Lazzara, J. Uitz, A. Bricaud, and L. Massi. 2017. On the discrimination of multiple phytoplankton groups from light absorption spectra of assemblages with mixed taxonomic composition and variable light conditions. Appl. Opt. **56**: 3952. doi:10.1364/AO.56.003952

Platt, T., and S. Sathyendranath. 2008. Ecological indicators for the pelagic zone of the ocean from remote sensing. Remote Sens. Environ. **112**: 3426–3436. doi:10.1016/j.rse.2007.10.016

Roesler, C., D. Stramski, E. J. D. Sa, R. Röttgers, and R. A. Reynolds. 2018. Chapter 5: Spectrophotometric measurements of particulate absorption using filter pads. *In* A. R. Neeley and A. Mannino [eds.], Ocean optics & biogeochemistry protocols for satellite ocean colour sensor validation, volume 1: Inherent optical property measurements and protocols: Absorption coefficient (v1.0). International Ocean Colour Coordinating Group (IOCCG) in collaboration with National Aeronautics and Space Administration (NASA).

Roesler, C. S., and M. J. Perry. 1995. In situ phytoplankton absorption, fluorescence emission, and particulate backscattering spectra determined from reflectance. J. Geophys. Res. **100**: 13279. doi:10.1029/95JC00455

Röttgers, R., and S. Gehnke. 2012. Measurement of light absorption by aquatic particles: Improvement of the quantitative filter technique by use of an integrating sphere approach. Appl. Opt. **51**: 1336. doi:10.1364/ao.51.001336

Sathyendranath, S., and others. 2020. Reconciling models of primary production and photoacclimation [Invited]. Appl. Opt. **59**: C100–C114. doi:10.1364/AO.386252

Schlüter, L., F. Møhlenberg, H. Havskum, and S. Larsen. 2000. The use of phytoplankton pigments for identifying and quantifying phytoplankton groups in coastal areas: Testing the influence of light and nutrients on pigment/chlorophyll a ratios. Mar. Ecol. Prog. Ser. **192**: 49–63. doi:10.3354/meps192049

Shen, F., R. Tang, X. Sun, and D. Liu. 2019. Simple methods for satellite identification of algal blooms and species using 10-year time series data from the East China Sea. Remote Sens. Environ. **235**: 111484. doi:10.1016/j.rse.2019.111484

Shi, W., and M. Wang. 2012. Satellite views of the Bohai Sea, Yellow Sea, and East China Sea. Prog. Oceanogr. **104**: 30–45. doi:10.1016/j.pocean.2012.05.001

Skákala, J., J. Bruggeman, R. J. W. Brewin, D. A. Ford, and S. Ciavatta. 2020. Improved representation of underwater light field and its impact on ecosystem dynamics: A study in the North Sea. J. Geophys. Res.: Oceans **125**: e2020JC016122. doi:10.1029/2020JC016122

Sun, D., W. Lai, S. Wang, Y. Huan, M. Bilal, Z. Qiu, and Y. He. 2019*a*. Synoptic relationships to estimate phytoplankton communities specific to sizes and species from satellite observations in coastal waters. Opt. Express **27**: A1156. doi:10.1364/OE.27.0A1156

Sun, X., F. Shen, R. J. W. Brewin, D. Liu, and R. Tang. 2019*b*. Twenty-year variations in satellite-derived chlorophyll-a and phytoplankton size in the Bohai Sea and Yellow Sea. J. Geophys. Res.: Oceans **124**: 8887–8912. doi:10.1029/2019JC015552

Sun, X., F. Shen, D. Liu, R. G. J. Bellerby, Y. Liu, and R. Tang. 2018. In situ and satellite observations of phytoplankton size classes in the entire continental shelf sea, China. J. Geophys. Res.: Oceans **123**: 3523–3544. doi:10.1029/2017JC013651

Swan, C. M., M. Vogt, N. Gruber, and C. Laufkoetter. 2016. A global seasonal surface ocean climatology of phytoplankton types based on CHEMTAX analysis of HPLC pigments. Deep-Sea Res. Part I: Oceanogr. Res. Pap. **109**: 137–156. doi:10.1016/j.dsr.2015.12.002

Torrecilla, E., D. Stramski, R. A. Reynolds, E. Millán-Núñez, and J. Piera. 2011. Cluster analysis of hyperspectral optical data for discriminating phytoplankton pigment assemblages in the open ocean. Remote Sens. Environ. **115**: 2578–2593. doi:10.1016/j.rse.2011.05.014

Uitz, J., H. Claustre, A. Morel, and S. B. Hooker. 2006. Vertical distribution of phytoplankton communities in open ocean: An assessment based on surface chlorophyll. J. Geophys. Res. **111**: doi:10.1029/2005JC003207

Uitz, J., D. Stramski, R. A. Reynolds, and J. Dubranna. 2015. Assessing phytoplankton community composition from hyperspectral measurements of phytoplankton absorption coefficient and remote-sensing reflectance in open-ocean environments. Remote Sens. Environ. **171**: 58–74. doi:10.1016/j.rse.2015.09.027

Vandermeulen, R. A., A. Mannino, A. Neeley, J. Werdell, and R. Arnone. 2017. Determining the optimal spectral sampling frequency and uncertainty thresholds for hyperspectral remote sensing of ocean color. Opt. Express **25**: A785. doi:10.1364/OE.25.00A785

Vidussi, F., H. Claustre, B. B. Manca, A. Luchetta, and J. Marty. 2001. Phytoplankton pigment distribution in relation to upper thermocline circulation in the eastern Mediterranean Sea during winter. J. Geophys. Res.: Oceans **106**: 19939–19956. doi:10.1029/1999jc000308

Wang, L., and others. 2016. Physical-biological coupling in the western South China Sea: The response of phytoplankton community to a mesoscale cyclonic eddy. PLoS One **11**: e153735. doi:10.1371/journal.pone.0153735

Werdell, P. J., and others. 2018. An overview of approaches and challenges for retrieving marine inherent optical

properties from ocean color remote sensing. Prog. Oceanogr. **160**: 186–212. doi:10.1016/j.pocean.2018.01.001

Werdell, P. J., and others. 2019. The plankton, aerosol, cloud, ocean ecosystem mission: Status, science, advances. Bull. Am. Meteor. Soc. **100**: 1775–1794. doi:10.1175/BAMS-D-18-0056.1

Wolanin, A., M. Soppa, and A. Bracher. 2016. Investigation of spectral band requirements for improving retrievals of phytoplankton functional types. Remote Sens. **8**: 871. doi:10.3390/rs8100871

Xi, H., M. Hieronymi, R. Röttgers, H. Krasemann, and Z. Qiu. 2015. Hyperspectral differentiation of phytoplankton taxonomic groups: A comparison between using remote sensing reflectance and absorption spectra. Remote Sens. **7**: 14781–14805. doi:10.3390/rs71114781

Zhang, H., E. Devred, A. Fujiwara, Z. Qiu, and X. Liu. 2018. Estimation of phytoplankton taxonomic groups in the Arctic Ocean using phytoplankton absorption properties: implication for ocean-color remote sensing. Opt. Express **26**: 32280. doi:10.1364/OE.26.032280

Zhang, J., D. Liu, P. Cao, Y. Wang, J. K. Keesing, J. Li, and L. Chen. 2016. A highly sensitive method for analyzing marker phytoplankton pigments: Ultra-high-performance liquid chromatography-tandem triple quadrupole mass spectrometry. Limnol. Oceanogr.: Methods **14**: 623–636. doi:10.1002/lom3.10117

Zhang, X., Y. Huot, A. Bricaud, and H. M. Sosik. 2015. Inversion of spectral absorption coefficients to infer phytoplankton size classes, chlorophyll concentration, and detrital matter. Appl. Opt. **54**: 5805. doi:10.1364/AO.54.005805

Zhou, W., G. Wang, C. Li, Z. Xu, W. Cao, and F. Shen. 2017. Retrieval of phytoplankton cell size from chlorophyll a specific absorption and scattering spectra of phytoplankton. Appl. Opt. **56**: 8362–8371. doi:10.1364/AO.56.008362

Zhu, Z., W. Ng, S. Liu, J. Zhang, J. Chen, and Y. Wu. 2009. Estuarine phytoplankton dynamics and shift of limiting factors: A study in the Changjiang (Yangtze River) Estuary and adjacent area. Estuar. Coast. Shelf Sci. **84**: 393–401. doi:10.1016/j.ecss.2009.07.005

Acknowledgments

The work is supported by NSFC project (No. 42076187) and ECNU Future Scientist project (WLKXJ2019-006). R.J.W. Brewin is supported by a UKRI Future Leader Fellowship (MR/V022792/1). In situ measurements were collected from the "Dongfanghong2" (2015-YS, 2016-YS, 2018-YS), "Zhehaike" (2016-CJ), and "Xiangyanghong18" (2018-ECS) research cruises, where all the scientists and crew members who participated in the field surveys are sincerely appreciated. We are grateful to Dongyan Liu and Richard G.J. Bellerby from SKLEC for HPLC pigments data of 2015-YS and 2016-YS, respectively. The authors greatly appreciate three anonymous reviewers and editors for their professional and constructive reviews. Datasets generated and analyzed which support the findings of this study are available at https://figshare.com/s/1795d92dd15bc143e720, but data share is not applicable. Data are available from the corresponding author upon request.

Conflict of Interest

None declared.

Submitted 30 April 2021
Revised 30 September 2021
Accepted 09 February 2022

Associate editor: David Antoine